Bundling in molecular dynamics simulations to improve generalization performance in high-dimensional neural network potentials

AUTHOR NAMES

Yasuharu Okamoto *

AUTHOR ADDRESS

†Data Platform Center, National Institute for Materials Science, 1-2-1 Sengen, Tsukuba, Ibaraki 305-0047, Japan

AUTHOR INFORMATION

Corresponding Author

Yasuharu Okamoto

ABSTRACT

We examined the influence of using bundling trajectories in molecular dynamics (MD) simulations for predicting energies in high-dimensional neural network potentials. In particular, we focused on the chemical transferability of gold nanoclusters, that is, how well the energy of gold clusters was estimated from the training data comprising gold clusters of different shapes and sizes. We observed that, as the number of MD simulations in the training data increased, the accuracy of the predicted energies improved.

Introduction

As an alternative to classical force field calculations, data-driven approaches such as high dimensional neural network potentials (HDNNP), [1–3] Gaussian approximation potentials (GAP), [4–7] and permutation invariant polynomials (PIP) [8–12] are drawing a great deal of interest because they can handle chemical reactions that include the formation and rupture of chemical bonds, which the typical classical force field methods fail to describe.[13] In addition, these approaches can achieve high accuracy if their training data are prepared using high level ab initio calculations instead of density functional theory (DFT) calculations. However, the chemical transferability of these approaches must still be established if they are to be widely used in practical problems. Here, chemical transferability implies predictability with respect to the data that differ from training data in machine learning. Because machine learning is an inductive and data-driven approach, it is ineffective for data that differ greatly from the training data; however, if it cannot be applied to data that differs slightly from the training data, it will lack practicality. HDNNP and GAP are advantageous as they can handle molecules with different numbers of atoms in one dataset. In contrast, PIP is suitable for applications involving a few many-body systems, such as the construction of global potential energy surfaces for chemical reactions in the gaseous phase.

It is noteworthy that, in the case of covalent bonding compounds such as organic molecules, recent studies showed promising results for chemical transferability. For example, the potential energy curves for the bond stretching and bending motions of a significantly large molecule (Fentanyl: $C_{22}H_{28}N_2O$) were reproduced fairly well from a training dataset comprising up to eight heavy atoms (C, N, and O) by utilizing HDNNP combined with normal mode sampling (NMS).[14] NMS is the superposition of randomly selected normal modes of a molecule up to a

given temperature T_{max} to generate distorted structures from the equilibrium geometry, which improves the chemical transferability of the dataset.

Nonetheless, it appears that there are still some aspects of the chemical transferability for noncovalent bonding compounds to be considered. Unlike covalent bonding compounds, where hybridized orbitals such as sp^3, sp^2, and sp effectively maintain the magnitude of bond angles and coordination numbers, metallic bonds do not show specific bond angles and coordination numbers.[15] This leads to great diversity with respect to the shape of metallic bonding compounds, which in turn makes the application of a data-driven approach more challenging. This is especially true for small metal clusters having multiple possible metastable structures that can be regarded as isomers with the same constituent number of atoms. Although the coordination number of the bulk metal is 8 or 12 in many cases, the coordination number of small clusters can range from 1 to 12. Thus, the chemical transferability in metallic bonding compounds should be examined because improving the generalization performance with data not included in the training dataset is essential to facilitate the widespread use of data-driven approaches. Thus, it is necessary to establish a data sampling scheme that can handle various structures of small metal clusters.

In this study, we investigated the chemical transferability in HDNNP with respect to small metal clusters. The training datasets were generated by bundling several trajectories obtained from MD simulations starting from each initial structure. We selected gold clusters as a test bed for this study. In particular, we focused on Au_{13}^+ and Au_{11}^+ clusters. Gilb et al reported 15 stable and metastable structures for both clusters.[16] Through ab initio calculations, they determined these structures to be consistent with cross section measurements. Their study was useful for generating various training and test data in this study. In addition, as the d orbitals of Au are fully occupied by electrons, we did not deem it necessary to consider mixed data on

high and low d-spin states. This is convenient for HDNNP, as the symmetry functions in HDNNP do not consider spin states.

Results and Discussion

A. Structures and relative energies of stable and metastable Au_{11}^+ and Au_{13}^+ clusters:

Gilb et al. reported 15 stable and metastable structures of Au_{11}^+ and Au_{13}^+ clusters obtained by quantum chemical calculations that were consistent with cross-section measurements.[16] They also reported the optimized atomic coordinates of these clusters, which were used as the initial geometries for our DFT calculations. The recalculated optimized structures are shown in Figs. S1 and S2 in the supporting information for the Au_{13}^+ and Au_{11}^+ clusters, respectively. S_0 was the most stable structure and M_1–M_{14} were the metastable structures. In ref. 16, a smaller number designating a cluster indicates a more stable structure. As metal bonds have high flexibilities, it is possible to adopt diverse structures that are clearly observed in Figs. S1 and S2. This diversity makes these clusters challenging for examining the chemical transferability of them. Figure 1 compares the calculated relative energies of 14 metastable states of Au_{11}^+ and Au_{13}^+ clusters with the values reported in ref. 16. Although the present calculations generally reproduced the Gilb's results, the values of M_3 and M_9 for Au_{13}^+ were less stable and the value of M_9 for Au_{11}^+ was more stable in this study than those in ref. 16. Calculations at the GGA level were performed in ref. 16, although different GGA functionals were used. In addition, ref. 16 used Gaussian basis functions in an isolated system, unlike this study, which utilized planewaves with periodic boundary conditions. These differences may cause subtle differences in the results of the relative energies.

B. Bundling MD trajectories to improve learning data:

First, learning data was generated from an MD simulation starting from the most stable structure S_0 of the Au_{13}^+ cluster to examine the ability of HDNNP to reproduce the energies of the metastable structures of M_1–M_{14} for the Au_{13}^+ cluster as test data. As shown in Fig. 2a, the energies predicted by HDNNP significantly deviated from those obtained by DFT. The mean absolute error (MAE) of 14 metastable structures is considerably high (0.409 eV), and the absolute error in M_8 is especially large (0.904 eV). Therefore, to generate a more effective dataset for training, we bundled two MD trajectories starting from the S_0 and M_8 structures of the Au_{13}^+ cluster. In this manner, the structure among the test data with the largest deviation from the DFT calculation was sequentially incorporated into the next training data. This operation was repeated three times, and Fig. 2b shows the results obtained by HDNNP, where the learning data was merged from the four MD trajectories starting from S_0, M_8, M_5, and M_{14}. The MAE of the energies of the eleven metastable structures that were not included in the training data was considerably improved (0.248 eV). However, there was still a significant difference of 0.883 eV in the M_{13} structure, where the HDNNP prediction exhibited the largest deviation from the DFT calculation. Moreover, by further increasing the number of structures included in the learning data where the MD trajectories starting from the eight structures of S_0, M_8, M_5, M_{14}, M_{13}, M_3, M_{10}, and M_{12} were bundled together, we observed that the DFT values of seven structures not included in the learning data were reproduced well, as shown in Fig. 2c. At this time, the MAE of the metastable structures that were not included in the training data was 0.106 eV, and the absolute error of the case with the largest deviation, M_{11}, was reduced to 0.180 eV.

Subsequently, we examined the total energy distribution obtained from 1, 4, 8, and 15 MD simulations as shown in Fig. 3. It is clear that only low energy range could be sampled in one

MD (S_0) simulation. Lower total energy means higher atomization energy. Thus, the energy distribution of 1 MD in Fig. 3 is consistent with Fig.2a. It was noteworthy that as the number of bundled MD simulations increased, the sampled energy range became wider and the energy distribution became more symmetrical. In addition, the energy distribution peak shifted to the higher energy. These changes appear to contribute to sample wider energy range thoroughly.

C. Prediction of energies of different cluster size:

The above results clearly show that the generalization performance will be improved if the learning data is composed of bundled MD trajectories starting from various structures. Therefore, to examine the generalization performance for more difficult problems, the energies of test data in which the number of atoms differs from that of the learning data were predicted by using HDNNP. Figure 4a shows the energies of 15 stable and metastable structures of Au_{11}^+ predicted by the learning data of bundled MD trajectories starting from 15 stable and metastable structures of Au_{13}^+. As will be explained in the computational details below, most of the influence caused by the difference between the number of atoms in the learning data and the test data can be treated by considering the atomization energy per atom. However, since subtle difference still remains in mean energy in Z-core normalization, it must be properly shifted. Ideally, it should be shifted such that the residual sum of squares between the true value and the predicted value is minimized. However, the assumption that all the true values of the test data are known is not realistic in practical applications. Thus, it should be fitted to a small number of values. As an example, the predicted value by HDNNP was shifted so that the energy of the most stable structure of Au_{11}^+ (i.e. S_0) coincided with the value obtained by DFT calculation. By considering the shift, it approaches the 45° line, which represents perfect fitting; however, it may be quantitatively insufficient. The MAEs for the 14 metastable structures of

Au_{11}^+ when shifted by minimizing the residual sum of squares and only by S_0 are 0.255 and 0.634 eV, respectively. It is noteworthy that the energy shift based on a few points strongly depends on the chosen points and requires attention.

Practically, it appears to be more interesting to examine the transferability when the number of atoms contained in the test data is larger than that in the training data. Figure 4b shows the HDNNP prediction of the energies of the 15 stable and metastable structures of Au_{13}^+ obtained by the learning data of bundled MD trajectories starting from the 15 stable and metastable structures of Au_{11}^+. When considering the shift by minimizing the residual sum of squares or the shift adjusted by S_0, the predicted values were close to the 45° line. The MAE for the shift by the residual sum of squares was 0.279 eV, whereas that for the shift by S_0 was 0.357 eV. In this case, the difference by the two shift methods is not so conspicuous.

D. Reproduction of different MD trajectories:

In the discussion so far, we have demonstrated that the generalization performance is improved by bundling MD trajectories that have various initial structures. However, the number of test data may be small and must be increased. Therefore, we examined the reproducibility of the energies along the MD trajectory which completely differed from the learning data. Although a cuboctahedron cluster composed of 13 Au atoms appears to be a common cluster structure as it is obtained by removing a part of a face-centered cubic crystal, the cluster is not included in the 15 stable and metastable structures of Au_{13}^+ identified by Gilb et al,[16] and it was not used as learning data in this study. MD calculation considering cuboctahedron as the initial structure was performed, and 200 structures were recorded every 50-time steps (0.0484 ps) as a test dataset. The energies of this test data were predicted by using two learning datasets that bundled 15 MD trajectories of Au_{13}^+ or Au_{11}^+. The results are shown in Fig. 5a and 5b. Note that in Fig.

5b ten data were selected for every 20 pieces of the test data and the predicted energies were shifted to minimize the residual sum of squares with respect to these ten data. When Au_{13}^{+} is used as the learning data, as the number of constituent atoms in the training and test data is identical, the predictions appear to be more accurate than in the case where Au_{11}^{+} is used as the learning data. Reflecting this, the MAE for the test data was 0.157 eV in the former and 0.189 eV in the latter. Although the accuracy of the latter was somewhat inferior, this result clearly indicates that it is possible to predict the energies along the MD trajectory of different numbers of atoms with a semi-quantitative accuracy. Judging from the magnitude of MAE, this result also suggests that the reproduction of the energies along the MD trajectory based on a single structure appears to be easier than that based on various metastable structures.

Conclusions

We studied data sampling schemes for HDNNP to predict the energies of gold clusters of different shapes and sizes. The motivation of our study was to clarify the chemical transferability of gold clusters, namely, how the energy of gold clusters was estimated from the training data comprising gold clusters of different shapes and sizes. We observed that, as the number of MD trajectories included in the training data increased, the accuracy of the predicted energies was significantly improved.

Computational Details

A. DFT calculations

All DFT calculations were performed using the Quantum Espresso (ver. 6.1) program package.[17] The generalized gradient approximation (GGA) of the exchange-correlation functional formulated by Perdew, Burke, and Ernzerhof (PBE96) was used for the

calculations.[18] Ultrasoft pseudopotential was employed for the Au atom in the calculations.[19] Plane-wave basis sets with cutoff energies of 30 and 300 Ry were used for the expansion of the wave functions and the charge density, respectively. Gamma-point sampling was utilized for Brillouin zone (BZ) integration. The Au_{11}^{+} and Au_{13}^{+} clusters were placed in a cubic supercell with 30 Bohr side, and a uniform background negative charge was added to preserve the charge neutrality of the supercell. MD simulations were performed at 1000 K by using the velocity scaling method. The time step of MD was 0.9676 fs.

B. HDNNP

HDNNP calculations were performed with a homemade program written in Python. In our HDNNP implementation, each constituent element in a molecule has its own neural network comprising three hidden layers with 150 nodes per layer. A rectified linear unit and a linear unit were used as the activation functions for the hidden and output layers, respectively. The loss function was calculated as the sum of the squared residuals between the DFT and the predicted energies. Training of the weights and biases in HDNNP was performed via the stochastic gradient descent method with a minibatch size of 200. The process was continued until 1000 epochs with a learning rate that gradually decreased in a stepwise manner from 0.00075 to 0.00025; thereafter, the results were recorded. We randomly divided learning data in a ratio of 9:1 for training and validation purposes, respectively. Furthermore, test data were added appropriately as described in the result and discussion section to evaluate the performance of the data sampling schemes.

In HDNNP, radial and angular symmetry functions are types of descriptors in a regression model. The radial symmetry function is a sum of the product of Gaussians given as follows:[3]

$$G_{rad}^{i} = \sum_{j=1}^{N_{atom}} e^{-\eta\left(R_{ij}-R_s\right)^2} f_c\left(R_{ij}\right) \qquad (1),$$

where η was fixed at 1.25 and the shifting parameter R_s was set to 55 values with equal intervals in the range of [0,9] Bohr. The function $f_c(R_{ij})$ was used as the cutoff for the interaction between long interatomic distances, and the form of the function is the same as that in Equation (6) of a review article by Behler.[3] The cutoff radius of the radial symmetry function was set to 14 Bohr,

We used an angular symmetry function with the following form:[3]

$$G_{ang}^{i} = 2^{1-\zeta} \sum_{j\neq i}^{N_{atom}} \sum_{k\neq i,j}^{N_{atom}} \left(1 + \lambda \cos\theta_{ijk}\right)^{\zeta} e^{-\eta\left(R_{ij}^2 + R_{ik}^2\right)} f_c\left(R_{ij}\right) f_c(R_{ik}), \quad (2)$$

where λ=±1, η was fixed at 0.1, and the set of exponents is ζ= {1, 1.2081, 1.4594, 1.7631, 2.13, 2.5733, 3.1088, 3.7557, 4.5372, 5.4814, 6.622, 8}. The cutoff radius of R_c in the angular symmetry function was set to 10 Bohr.

In machine learning, data are usually standardized to improve robustness against outliers. The following Z-core normalization is the most popular standardization procedure and was used in this study, where the original energy E is converted into E'as follows:

$$E' = (E - \mu) / \sigma \quad (3)$$

where μ and σ are the mean and standard deviation of E, respectively. When the total energy of the cluster is used as E, and if the cluster sizes of the learning data (= training plus validation data) and the test data are different, for example, Au_{13}^+ and Au_{11}^+ clusters are used for learning data and test data, respectively, the average energy of the Au_{13}^+ cluster will be used to predict the energy of the Au_{11}^+ cluster. This results in poor prediction performance because the energy difference due to the difference in the number of atoms (11 and 13) is much larger than the change of energies due to the structural displacement for the same number of atoms. Therefore, to reduce the influence of the difference of the number of atoms, the atomization energy per atom defined by the following formula was used as E:

$$E = E_{tot}(Au_n^+)/n - E_{tot}(Au) \quad (4)$$

Here, n is the number of atoms in the cluster, and E_{tot} (Au_n^+) and E_{tot} (Au) represent the total energies of the Au_n^+ cluster and of the energy one Au atom, respectively.

C. Bundling of MD trajectories

The learning data was prepared by performing the MD simulations as described above with 15 stable and metastable Au_{11}^+ and Au_{13}^+ clusters as the initial structures. To properly describe these initial structures, all the structures in the first 50 MD steps from the start of the simulation were included in the data; subsequently, the structure was sampled every 50 steps to gather various structures when possible. Starting from the most stable structure S_0, metastable structures were sequentially added to the learning data. When the learning data comprised N_{st} MD trajectories, we set each trajectory to be selected with a probability of $1/N_{st}$. In most cases, the number of learning data (N_{data}) was set as N_{data} = 4000. However, N_{data} = 3000 was used when N_{st} = 1 (Figure 2a), and N_{data} = 8000 was used for the reproduction of the MD trajectory (Figure 5a and 5b).

Associated Content

Supporting Information. The following file, provided as Figures S1 and S2, is available free-of-charge as a supporting information.

Author Information

Authors' E-mail address

okamoto.yasuharu@nims.go.jp

ORCID

Yasuhau Okamoto : 0000-0001-6751-2447

Author Contributions

Y.O. performed all calculations and the analysis of the results.

Notes

The authors declare no competing financial interests.

REFERENCES

(1) Yao, K.; Herr, J. E.; Toth, D. W.; McKintyre, R.; Parkhill, J. The TensorMol-0.1 model chemistry: A neural network augmented with long-range physics. *Chem. Sci.* **2018**, *9* (8), 2261–2269.

(2) Behler, J. First Principles Neural Network Potentials for Reactive Simulations of Large Molecular and Condensed Systems. *Angew. Chemie - Int. Ed.* **2017**, *56* (42), 12828–12840.

(3) Behler, J. Constructing high-dimensional neural network potentials: A tutorial review. *Int. J. Quantum Chem.* **2015**, *115* (16), 1032–1050.

(4) Bartók, A. P.; Payne, M. C.; Kondor, R.; Csányi, G. Gaussian approximation potentials: The accuracy of quantum mechanics, without the electrons. *Phys. Rev. Lett.* **2010**, *104* (13), 1–4.

(5) Szlachta, W. J.; Bartók, A. P.; Csányi, G. Accuracy and transferability of Gaussian approximation potential models for tungsten. *Phys. Rev. B - Condens. Matter Mater. Phys.* **2014**, *90* (10), 1–6.

(6) Bartok, A. P.; De, S.; Poelking, C.; Bernstein, N.; Kermode, J.; Csanyi, G.; Ceriotti, M. Machine Learning Unifies the Modelling of Materials and Molecules. **2017**, No. December, 1–9.

(7) Gillan, M. J.; Alfè, D.; Bartók, A. P.; Csányi, G. First-principles energetics of water clusters and ice: A many-body analysis. *J. Chem. Phys.* **2013**, *139* (24).

(8) Jiang, B.; Guo, H. Permutation invariant polynomial neural network approach to fitting potential energy surfaces. III. Molecule-surface interactions. *J. Chem. Phys.* **2014**, *141* (3).

(9) Xie, Z.; Bowman, J. M. Permutationally invariant polynomial basis for molecular energy surface fitting via monomial symmetrization. *J. Chem. Theory Comput.* **2010**, *6* (1), 26–34.

(10) Zhou, X.; Nattino, F.; Zhang, Y.; Chen, J.; Kroes, G. J.; Guo, H.; Jiang, B. Dissociative chemisorption of methane on Ni(111) using a chemically accurate fifteen dimensional potential energy surface. *Phys. Chem. Chem. Phys.* **2017**, *19* (45), 30540–30550.

(11) Li, J.; Jiang, B.; Guo, H. Permutation invariant polynomial neural network approach to fitting potential energy surfaces. II. Four-atom systems. *J. Chem. Phys.* **2013**, *139* (20), 1–8.

(12) Ayouz, M.; Babikov, D. Global permutationally invariant potential energy surface for ozone forming reaction. *J. Chem. Phys.* **2013**, *138* (16).

(13) Van Duin, A. C. T.; Dasgupta, S.; Lorant, F.; Goddard, W. A. ReaxFF: A reactive force field for hydrocarbons. *J. Phys. Chem. A* **2001**, *105* (41), 9396–9409.

(14) Smith, J. S.; Isayev, O.; Roitberg, A. E. ANI-1: an extensible neural network potential with DFT accuracy at force field computational cost. *Chem. Sci.* **2017**, *8* (4), 3192–3203.

(15) Atkins, Peter, Overton, Tina, Rourke, Jonathan, Weller, Mark, Armstrong, F. *Shriver and Atkins' Inorganic Chemistry*, 5th editio.; OUP Oxford, 2009.

(16) Gilb, S.; Weis, P.; Furche, F.; Ahlrichs, R.; Kappes, M. M. Structures of small gold cluster cations (Aun+, n<14): Ion mobility measurements versus density functional calculations. *J. Chem. Phys.* **2002**, *116* (10), 4094–4101.

(17) Giannozzi, P.; Baroni, S.; Bonini, N.; Calandra, M.; Car, R.; Cavazzoni, C.; Ceresoli, D.; Chiarotti, G. L.; Cococcioni, M.; Dabo, I.; et al. QUANTUM ESPRESSO: A modular and open-source software project for quantum simulations of materials. *J. Phys. Condens. Matter* **2009**, *21* (39).

(18) Perdew, J. P.; Burke, K.; Ernzerhof, M. Generalized gradient approximation made simple. *Phys. Rev. Lett.* **1996**, *77* (18), 3865–3868.

(19) Laasonen, K.; Car, R.; Lee, C.; Vanderbilt, D. Implementation of ultrasoft pseudopotentials in ab initio molecular dynamics. *Phys. Rev. B* **1991**, *43* (8), 6796–6799.

Figure Captions

Figure 1 Calculated relative energies of 14 metastable states of Au_{11}^+ and Au_{13}^+ clusters compared to the most stable structure S_0. The results were compared with the values in ref. 16.

Figure 2 Scatter plot of prediction by HDNNP versus DFT calculation with respect to the atomization energy of Au_{13}^+ clusters. a) only S_0 in Fig. S1 was used as an initial structure of MD simulation to generate learning data. b) Four structures (S_0, M_9, M_5, and M_{14}) were used as initial structures of MD simulations to generate learning data. c) Eight structures (S_0, M_9, M_5, M_{14}, M_{13}, M_3, M_{10}, and M_{12}) were used as initial structures of MD simulations to generate learning data.

Figure 3 Total energy distribution of 1 MD trajectory based on S_0 structure, 4 MD trajectories based on S_0, M_9, M_5, and M_{14} structures, 8 MD trajectories based on S_0, M_9, M_5, M_{14}, M_{13}, M_3, M_{10}, and M_{12} structures, and 15 MD trajectories based on S_0, and M_1-M_{14} structures.

Figure 4 Scatter plot of prediction by HDNNP versus DFT calculation with respect to the atomization energy of clusters of different sizes. a) Energies of Au_{11}^+ predicted from the learning data comprising 15 structures of Au_{13}^+ (S_0, and M_1-M_{14} in Fig. S1). b) Energies of Au_{13}^+ predicted from the learning data comprising 15 structures of Au_{11}^+ (S_0, and M_1-M_{14} in Fig. S2).

Figure 5 Reproduction of atomization energies along MD trajectories starting from the cuboctahedron Au_{13}^+ cluster. Note that as ΔE(=E[HDNNP]-E[DFT]) is multiplied by 13.6, this corresponds to electron volt units. a) Energies predicted from the learning data comprising 15 structures of Au_{13}^+ (S_0, and M_1-M_{14} in Fig. S1). b) Energies predicted from the learning data comprising 15 structures of Au_{11}^+ (S_0, and M_1-M_{14} in Fig. S2).

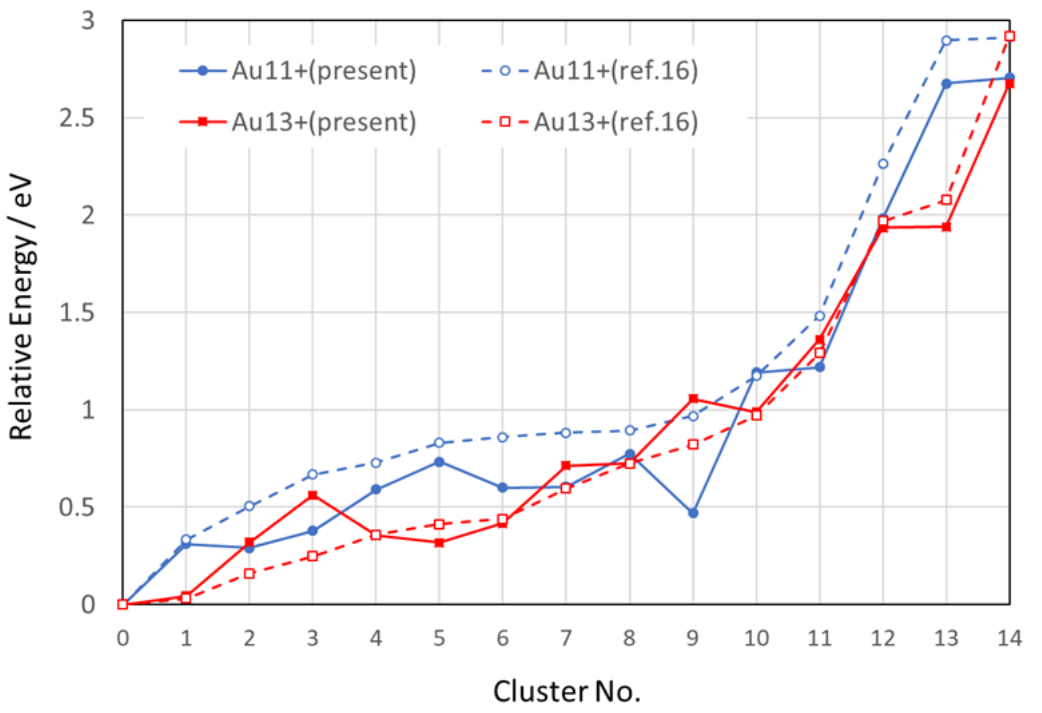
Au11+(present)
Au11+(ref.16)
Au13+(present)
Au13+(ref.16)
Relative Energy / eV
Cluster No.
0
0.5
1
1.5
2
2.5
3
0
1
2
3
4
5
6
7
8
9
10
11
12
13
14

Figure 1

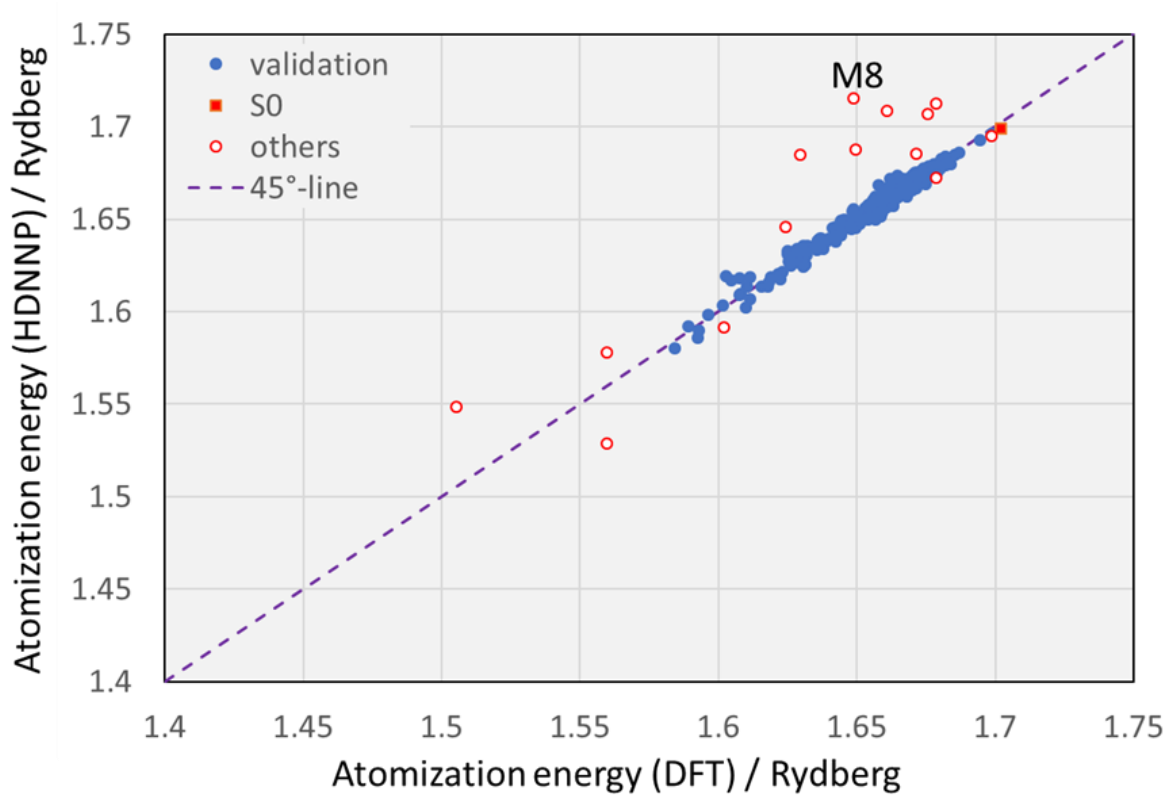

Figure 2a

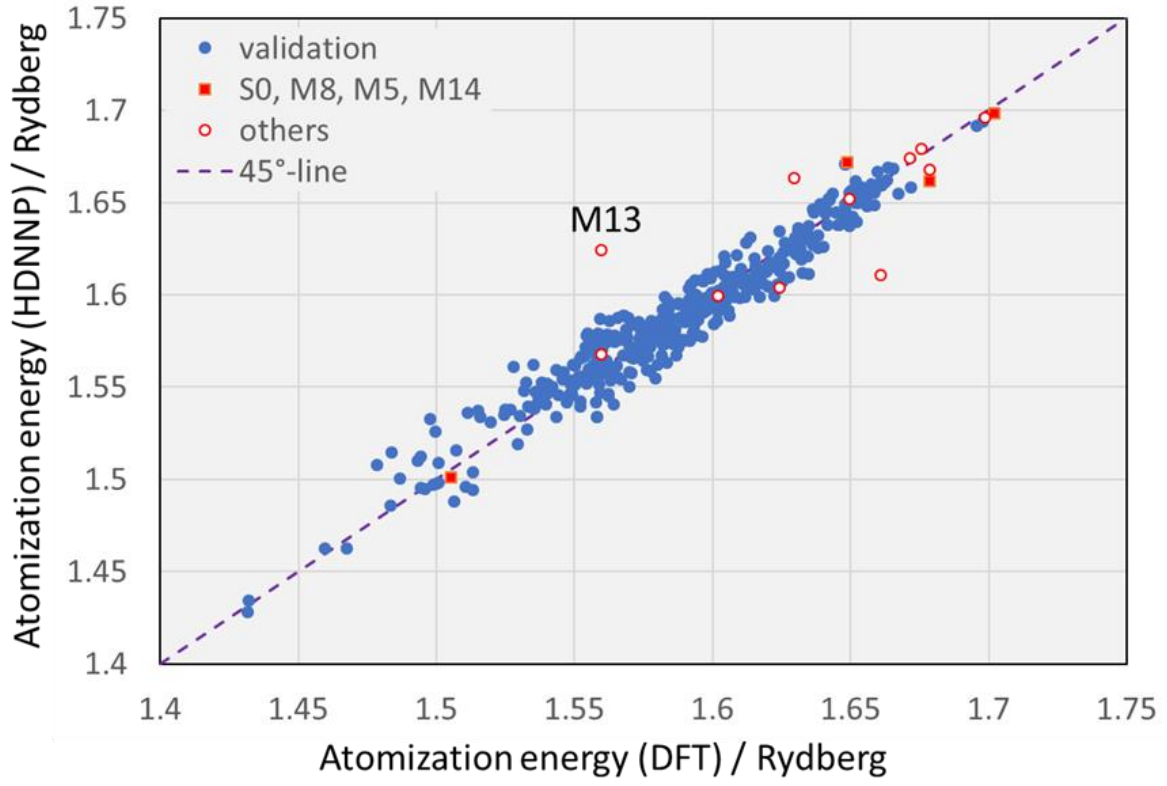

Figure 2b

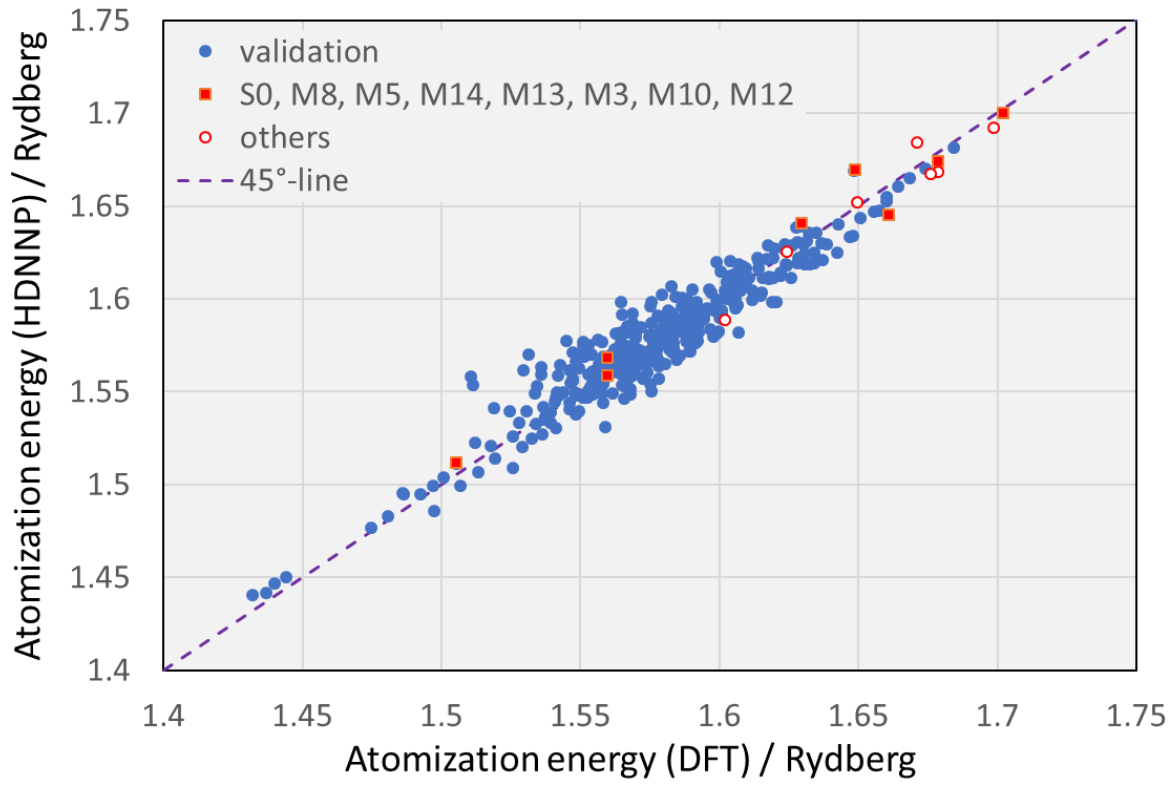
validation
S0, M8, M5, M14, M13, M3, M10, M12
others
45°-line
Atomization energy (HDNNP) / Rydberg
Atomization energy (DFT) / Rydberg
1.4
1.45
1.5
1.55
1.6
1.65
1.7
1.75

Figure 2c

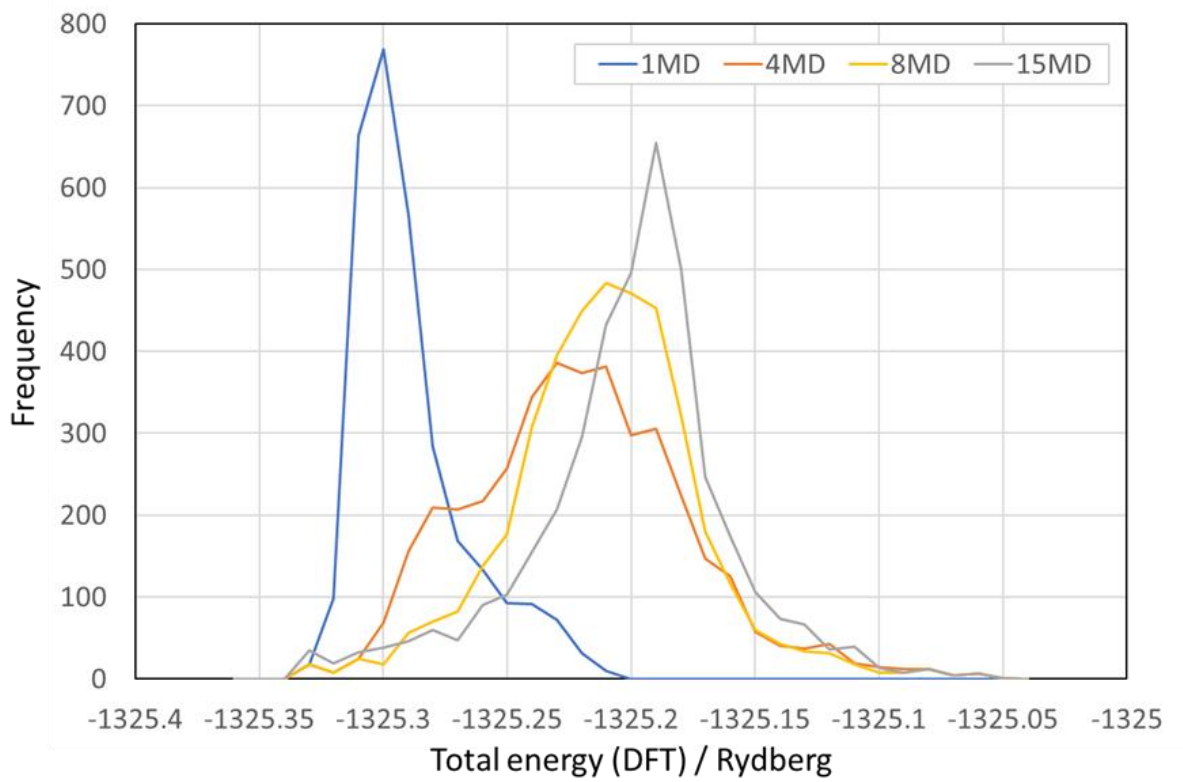
800
700
600
500
400
300
200
100
0
Frequency
1MD
4MD
8MD
15MD
-1325.4
-1325.35
-1325.3
-1325.25
-1325.2
-1325.15
-1325.1
-1325.05
-1325
Total energy (DFT) / Rydberg

Figure 3

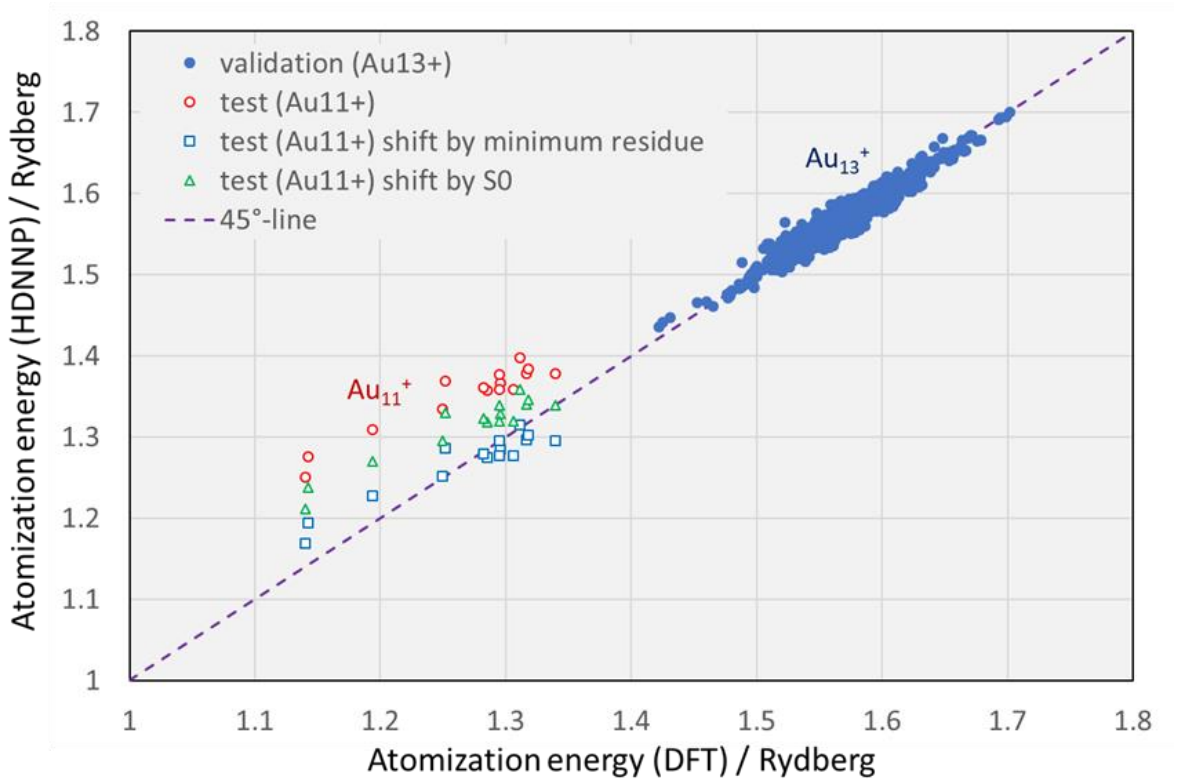

Figure 4a

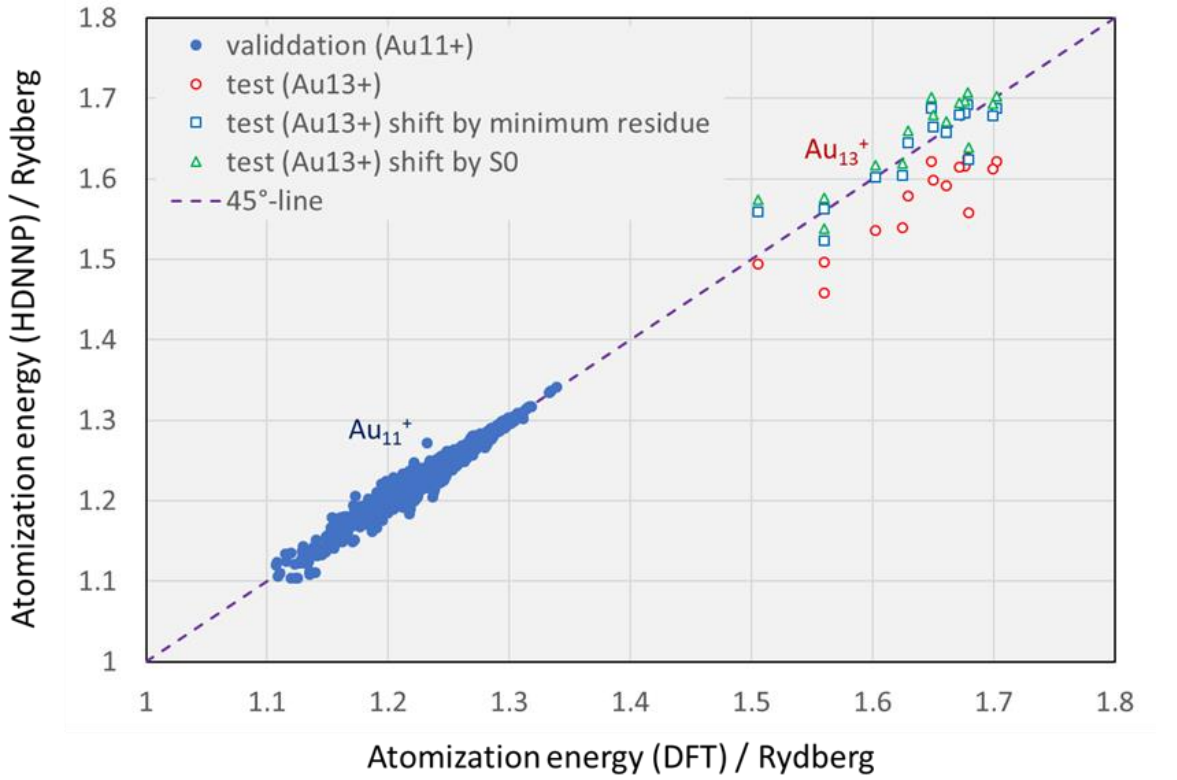

Figure 4b

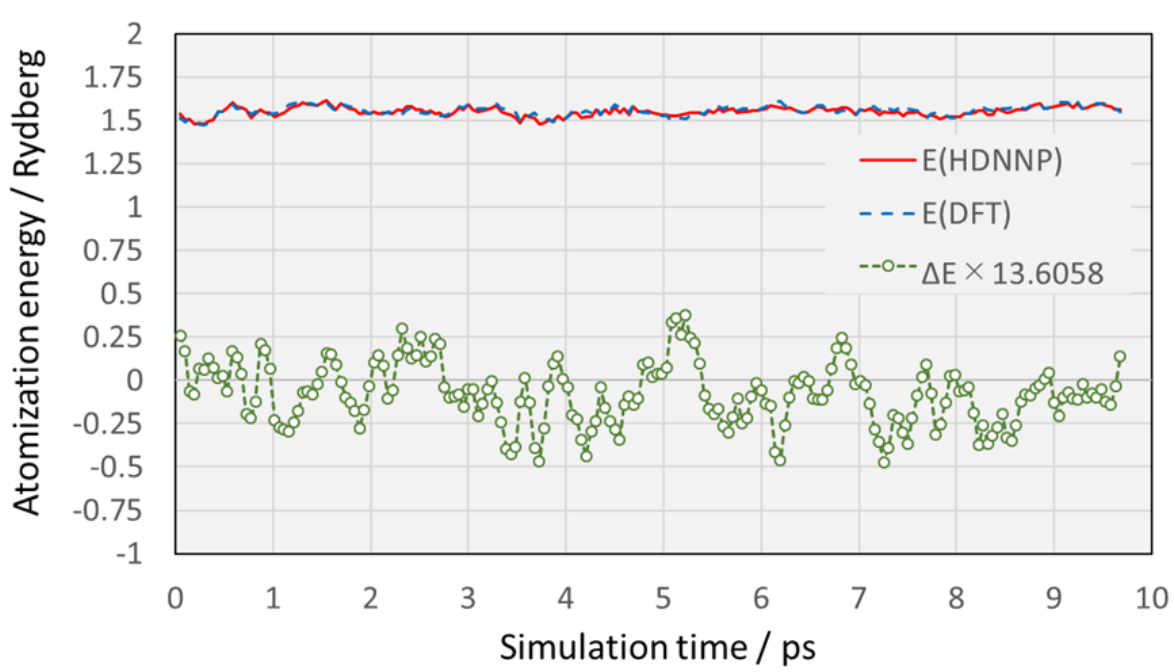

Figure 5a

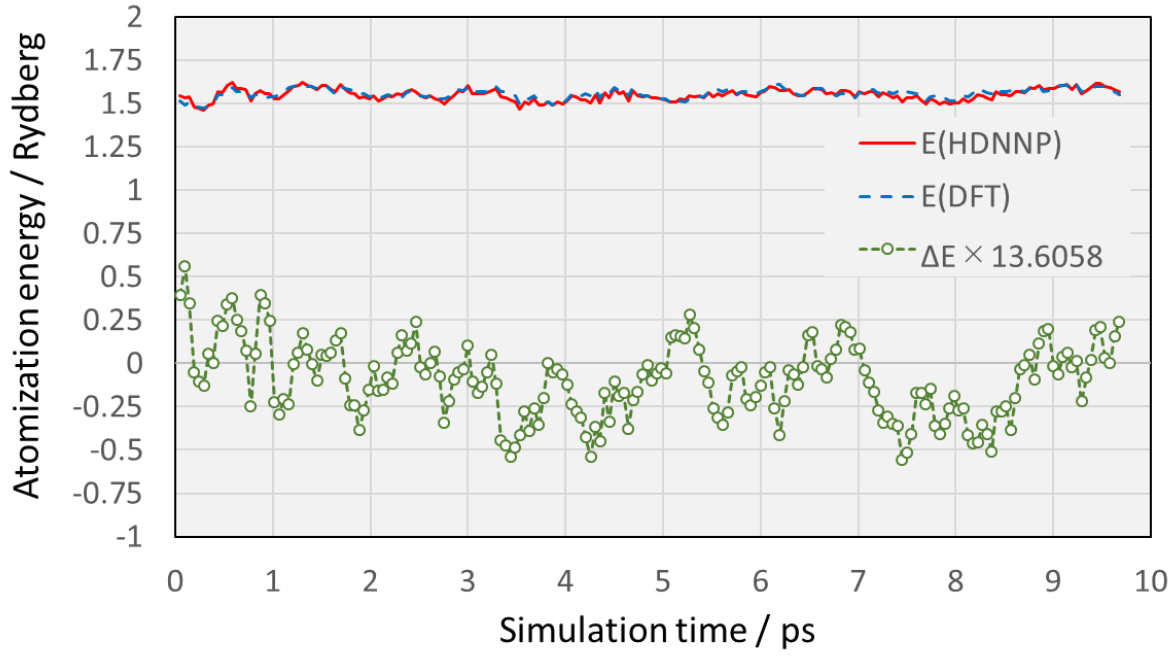

Figure 5b

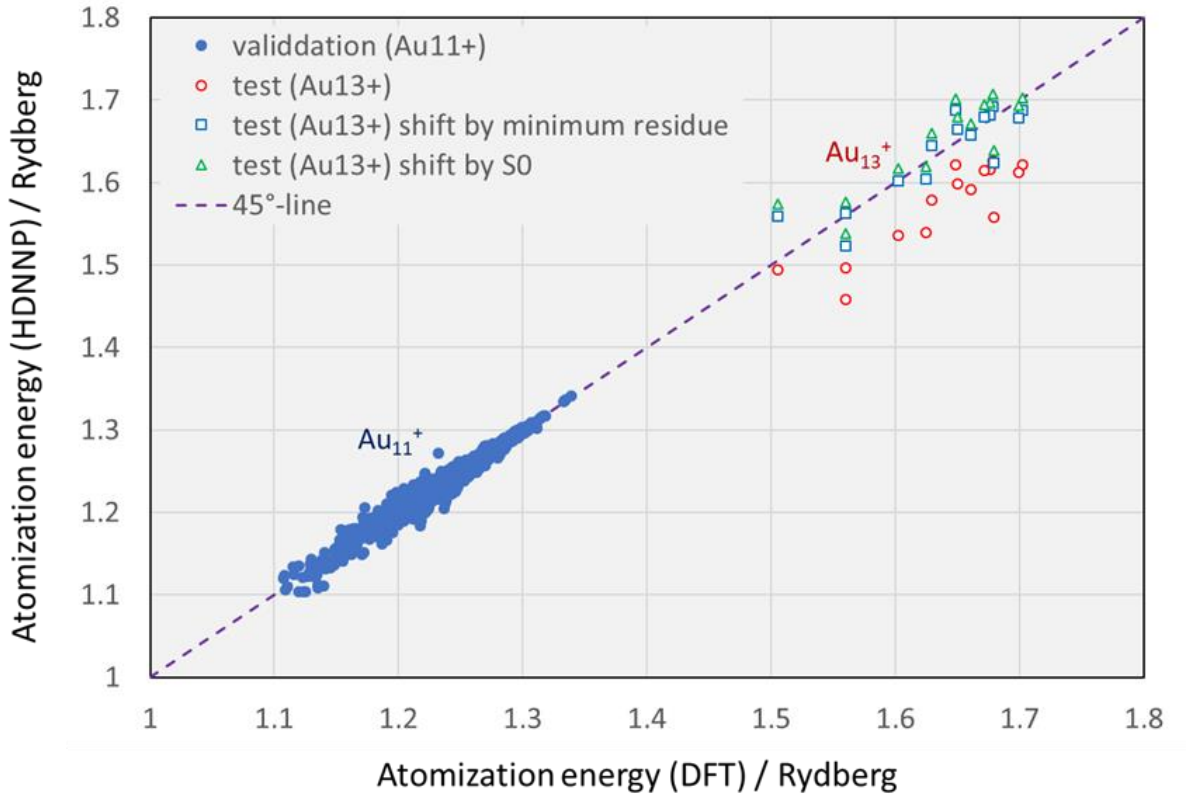
validdation (Au11+)
test (Au13+)
test (Au13+) shift by minimum residue
test (Au13+) shift by S0
45°-line
Au11+
Au13+
Atomization energy (HDNNP) / Rydberg
Atomization energy (DFT) / Rydberg
1.8
1.7
1.6
1.5
1.4
1.3
1.2
1.1
1
1
1.1
1.2
1.3
1.4
1.5
1.6
1.7
1.8

TOC